Continuity Order of Local Displacement in Volumetric Image Sequence

Koji Kashu[1], Yusuke Kameda[2], Masaki Narita[1],
Atsushi Imiya[3], and Tomoya Sakai[3]

[1] School of Advanced Integration Science, Chiba University
[2] JSPS/School of Advanced Integration Science, Chiba University
[3] Institute of Media and Information Technology, Chiba University
Yayoi-cho 1-33, Inage-ku, Chiba, 263-8522, Japan

Abstract. We introduce a method for volumetric cardiac motion analysis using variational optical flow computation involving the prior with the fractional order differentiations. The order of the differentiation of the prior controls the continuity class of the solution. Fractional differentiations is a typical tool for edge detection of images. As a sequel of image analysis by fractional differentiation, we apply the theory of fractional differentiation to a temporal image sequence analysis. Using the fractional order differentiations, we can estimate the orders of local continuities of optical flow vectors. Therefore, we can obtain the optical flow vector with the optimal continuity at each point.

1 Introduction

As an application of the computer vision technique to clinical biomechanical motion analysis from volumetric image sequences, we deal with spatial optical flow computation for the beating heart. In recent years, it is possible to measure a series of volumetric cardiac images dynamically using MRI, Cine X-ray CT, and Ultrasonic imaging and so on. The most important physical natures of the cardiac optical flow computation are that the motion of the beating heart is spatial dynamics and the heart wall is deformable [1,7]. For registration of temporal volumetric cardiac images, optical flow is a fundamental feature to express temporal deformation. Therefore, accurate computation of optical flow field and segmentation of optical flow fields are essential tasks for pre-processing to temporal registration of cardiac image sequence.

The prior terms of variational optical flow and variationl image registration control local continuity orders of small displacements in images of a spatiotemporal image sequence and deformation for images from an atlas image. In this paper, we introduce an estimation method for the optimal continuity order of local small displacements of image sequence. The continuity order of local displacement is computed using variational optical flow computation with the prior which involves the fractional order differentiation [2,3,4,5] of the displacement field. We

B. Fischer, B. Dawant, and C. Lorenz (Eds.): WBIR 2010, LNCS 6204, pp. 48–59, 2010.

apply local continuity estimation to volumetric cardiac optical flow computation. The prior term with the first-order derivatives is a common regularizer in optical-flow computation [8]. The prior term with the second-order derivatives, of which the origin in mechanics goes back to Kirchhoff [10] on the elastic theory, is a common regularizer in boundary extraction for tracking of the object-boundary and warping [11] in computational anatomy. From the viewpoint of the order of derivatives in the regularizers for the optical-flow computation, the Horn-Schunck [9] and the deformable-model [6] constraints require that the solution is a continuous twice differentiable function and a continuous four-time differentiable function, respectively. The order of the differentiations in the prior controls the continuity class of the solution. Therefore, by selecting an appropriate order of the differentiation in the prior of variational optical flow computation, we can estimate motion boundary and classify the continuity order of the motion field.

Total variational (TV) regularization is a successful method of optical flow computation of an image sequence with discontinuity of the gray values and motion field. TV regularization uses the total variation of optical flow field as the prior, although the classical Horn-Schunck method [9] uses the L_2 norm of the gradient of flow field. TV regularization optical flow computation [22] derives a nonlinear elliptic partial differential equation as the Euler-Lagrange equation of the energy functional of the problem. The generalization of the order of differentiation in a Horn-Schunck-type prior is another modification of the original Horn-Schunck regularization, since this generalization yields a linear Euler-Lagrange equation [4,5]. There are two types of generalization of the differentiations in priors; the first one deals with higher-order differentiations, and the second one deals with fractional order differentiations. We focus on the second type of generalization, that is, we deal with the variational optical flow computation with a prior term involves a fractional order differentiation of optical flow vectors.

Recently, fractional partial differential equations have been widely used in various areas of science and engineering, because fractional differential equations describe diffusion and wave propagation in inhomogeneous media and fractal structures [18,20]. As a sequel, we propose variational optical flow computation involving the prior with fractional order differentiations on optical flow vectors. A definition of fractional differentiation is based on the Fourier transform of differential operations, which is easily implemented using the first Fourier transform and the filter theory [2]. We solve the spatially fractional partial differential equation using the Fourier transform method to compute fractional derivatives. Since fractional differentiations[1] are linear operations, the fractional order regularization for optical flow computation [22] derives a linear fractional order elliptic partial differential equation as the Euler-Lagrange equation of the

[1] The definitions of fractional derivative are

$$\frac{d^\alpha}{dx^\alpha} f(x) = \frac{1}{\Gamma(n-\alpha)} \frac{d^n}{dx^n} \int_0^t (t-\tau)^{n-\alpha-1} f(\tau) d\tau.$$

Therefore, the relations $\frac{d^{1/2}}{dx^{1/2}} x = \frac{1}{\sqrt{2\pi}} x^{1/2}$ and $\frac{d^{1/2}}{dx^{1/2}} \frac{1}{\sqrt{2\pi}} x^{1/2} = 1$ are satisfied.

energy functional. Therefore, we can numerically solve the problem using the same strategy that is used to solve the Horn-Schunck method.

2 Fractional Optical Variational Problem

2.1 Fractional Order Differentiations

Using the Fourier transform pair

$$F(\boldsymbol{\xi}) = \frac{1}{(2\pi)^{3/2}} \int_{\mathbf{R}^3} f(\boldsymbol{x}) e^{-i(\boldsymbol{x}^\top \boldsymbol{\xi})} d\boldsymbol{x}, \tag{1}$$

$$f(\boldsymbol{x}) = \frac{1}{(2\pi)^{3/2}} \int_{\mathbf{R}^3} F(\boldsymbol{\xi}) e^{i(\boldsymbol{x}^\top \boldsymbol{\xi})} d\boldsymbol{\xi}, \tag{2}$$

for $\boldsymbol{x} = (x, y, z)^\top$ and $\boldsymbol{\xi} = (\xi, \eta, \zeta)^\top$, we define the operations Λ

$$\Lambda f(\boldsymbol{x}) = \frac{1}{(2\pi)^{3/2}} \int_{\mathbf{R}^{3/2}} |\boldsymbol{\xi}| F(\boldsymbol{\xi}) e^{i(\boldsymbol{x}^\top \boldsymbol{\xi})} d\boldsymbol{\xi}. \tag{3}$$

We have the equality

$$\int_{\mathbf{R}^3} |\nabla f|^2 d\boldsymbol{x} = \int_{\mathbf{R}^3} |\Lambda f|^2 d\boldsymbol{x}, \tag{4}$$

since

$$\int_{\mathbf{R}^3} |f|^2 d\boldsymbol{x} = \int_{\mathbf{R}^3} |F|^2 d\xi d\boldsymbol{\xi}. \tag{5}$$

2.2 Variationl Image Analysis

For the positive integer $n \geq 1$, setting the operator D^n to be

$$D^{n+1} f = \begin{pmatrix} \partial_x D^n f \\ \partial_y D^n f \\ \partial_z D^n f \end{pmatrix}, \; Df = \nabla f = \begin{pmatrix} \partial_x f \\ \partial_y f \\ \partial_z f \end{pmatrix}, \tag{6}$$

we define the operation

$$|T^\alpha f|^2 = \begin{cases} |D^\alpha f|^2, \text{ if } \alpha \text{ is an integer,} \\ |\Lambda^\alpha f|^2, \text{ otherwise.} \end{cases} \tag{7}$$

As a generalization of the Horn-Schucnk method [9] such that

$$H(\boldsymbol{u}) = \int_{\mathbf{R}^3} \left\{ (\nabla f^\top \boldsymbol{u} + \partial_t f)^2 + \kappa(|\nabla u|^2 + |\nabla v|^2 + |\nabla w|^2) \right\} d\boldsymbol{x}, \tag{8}$$

we deal with the variational energy functional

$$J_\alpha(\boldsymbol{u}) = \int_{\mathbf{R}^3} \{ D(f, \boldsymbol{u})^2 + \kappa(|T^\alpha u|^2 + |T^\alpha v|^2 + |T^\alpha w|^2) \} d\boldsymbol{x}, \tag{9}$$

where $\kappa \geq 0$ and $\alpha = n + \varepsilon$ where $0 < \varepsilon < 1$ and n is a non-negative integer for $\boldsymbol{u} = (x, y, z)^\top$. Since $\Lambda = \Lambda^*$, the Euler-Lagrange equation and the associated diffusion equation of eq. (9) are

$$\Lambda^{2\alpha}\boldsymbol{u} + \frac{1}{\kappa}D(f, \boldsymbol{u})\nabla_{\boldsymbol{u}}D(f, \boldsymbol{u}) = 0, \tag{10}$$

$$\partial_\tau \boldsymbol{u} = (-\Lambda^{2\alpha})\boldsymbol{u} - \frac{1}{\kappa}D(f, \boldsymbol{u})\nabla_{\boldsymbol{u}}D(f, \boldsymbol{u}), \tag{11}$$

where $\nabla_{\boldsymbol{u}}$ is the gradient with respect to $\boldsymbol{u}$ and ∂_τ is the partial derivative with respect to τ. For variational optical flow computation and variational image registration, the first term of eq. (9) is

$$D(f, \boldsymbol{u}) = \nabla f^\top \boldsymbol{u} + f_t = f_x u + f_y v + f_z w + f_t \tag{12}$$

for a spatiotemporal image sequence $f(\boldsymbol{x}, t)$ and

$$D(f, \boldsymbol{u}) = g(\boldsymbol{x}) - f(\boldsymbol{x} + \boldsymbol{u}) \tag{13}$$

for a pair of given functions g and f, respectively. Equation (10) coincides with the Euler-Lagrange equation of the Horn-Schunck method and the deformable-model method for $\alpha = 1$ and $\alpha = 2$, respectively, if the function $D(f, \boldsymbol{u})$ in the first term of eq. (9) is given by eq. (12). Furthermore, for variational image registration, we have

$$\Lambda^{2\alpha}\boldsymbol{u} - \frac{1}{\kappa}(g(\boldsymbol{x}) - f(\boldsymbol{x} + \boldsymbol{u}))\nabla f(\boldsymbol{x} + \boldsymbol{u}) = 0. \tag{14}$$

Therefore, if $\alpha = 1$ and $\alpha = 2$, the prior term of eq. (9) is that of diffusion registration and curvature registration, respectively [15].

2.3 Selection of Order of Prior

The solution involving the lth-order prior is

$$\boldsymbol{u}(x, y, z) = \begin{pmatrix} u \\ v \\ w \end{pmatrix} = \begin{pmatrix} \sum_{i,j,k=0}^{l-1} a_{ijk} x^i y^j z^k \\ \sum_{i,j,k=0}^{l-1} b_{ijk} x^i y^j z^k \\ \sum_{i,j,k=0}^{l-1} c_{ijk} x^i y^j z^k \end{pmatrix} \tag{15}$$

for nonnegative integers k, that is, the solution is locally a $(k-1)$th-order polynomial of x and y. This property implies that the priors involving the first- and second-order differentiations derive a piecewise linear and affine optical flow, respectively.

Let $\boldsymbol{u}(x, y, t; \alpha)$ be the optical flow vector computed for fixed α. For each point $\boldsymbol{x}$, we select

$$\boldsymbol{u}^*(x, y, t; \alpha^*) = arg\min_{\alpha} F(\boldsymbol{u}; \alpha, \kappa),\ \alpha^*(x, y, t) = arg\min F(\boldsymbol{u}; \alpha, \kappa) \tag{16}$$

where

$$F(\boldsymbol{u};\alpha,\kappa) = D(f,\boldsymbol{u})^2 + \kappa(|T^\alpha u|^2 + |T^\alpha v|^2 + |T^\alpha w|^2) \tag{17}$$

for a predetermined positive parameter κ as the solution vector of point $\boldsymbol{x}$. Equation (16) estimates the local continuity order of the optical flow vector, that is, point $\boldsymbol{x}$ with the optical flow vector $\boldsymbol{u}(x,y,t;\alpha)$ is the class $(\alpha-1)$ function of $\boldsymbol{x}$. We call $\alpha^* = \alpha(\boldsymbol{x},t)$, which establishes the minimum of eq. (16), the α-map [21] of the optical flow field (α-map in abbreviation.).

Using α-map, we construct a two-path algorithm such that

1. Let α_0 and α_1 be a pair of constants such that $\alpha_0 < \alpha_1$. Compute optical flow for each α for $\alpha_0 \le \alpha \le \alpha_1$ and construct α-map $\alpha^*(\boldsymbol{x})$.
2. Compute displacement field $\boldsymbol{u}^{**}(\boldsymbol{x})$ for point $\boldsymbol{x}$ as the solution of the equation

$$\partial_\tau \boldsymbol{u} = -\Lambda^{2\alpha^*(\boldsymbol{x})}\boldsymbol{u} - \frac{1}{\kappa}D(f,\boldsymbol{u})\nabla_{\boldsymbol{u}}D(f,\boldsymbol{u}). \tag{18}$$

3 Numerical Examples

3.1 Discretization of Equation

From eq. (11), we have semi-explicit discretizations such that

$$\frac{\boldsymbol{u}_{kmn}^{(l+1)} - \boldsymbol{u}_{kmn}^{(l)}}{\Delta\tau} = (-\Lambda^{2\alpha})\boldsymbol{u}_{kmn}^{(l)} - \frac{1}{\kappa}D(f,\boldsymbol{u}_{kmn}^{(l+1)})\nabla_{\boldsymbol{u}}D(f,\boldsymbol{u}_{kmn}^{(l+1)}), \tag{19}$$

$$\frac{\boldsymbol{u}_{kmn}^{(l+1)} - \boldsymbol{u}_{kmn}^{(l)}}{\Delta\tau} = (-\Lambda^{2\alpha})\boldsymbol{u}_{kmn}^{(l+1)} - \frac{1}{\kappa}D(f,\boldsymbol{u}_{kmn}^{(l)})\nabla_{\boldsymbol{u}}D(f,\boldsymbol{u}_{kmn}^{(l)}). \tag{20}$$

3.2 Numerical Computation

We evaluate numerical performances of the fractional order derivative in the prior for volumetric cardiac optical flow computation. Equation (19) derives the iteration form [14]

$$(\boldsymbol{I} + \frac{\Delta\tau}{\kappa}\boldsymbol{S}_{kmn})\boldsymbol{u}_{kmn}^{(l+1)} = \boldsymbol{u}_{kmn}^{(l)} + \Delta\tau(-\boldsymbol{\Lambda}^{2\alpha})\boldsymbol{u}_{kmn}^{(l)} - \frac{\Delta\tau}{\kappa}\boldsymbol{c}_{kmn},\ l \ge 0 \tag{21}$$

for the numerical computation of α optical flow, where

$$\boldsymbol{S}_{kmn} = (\nabla f)_{kmn}(\nabla f)_{kmn}^\top,\ \ \boldsymbol{c}_{kmn} = (\partial_t f)_{kmn}(\nabla f)_{kmn}. \tag{22}$$

The numerical Fourier transform achieves the operation $(-\Lambda^{2\alpha}\boldsymbol{u})_{kmn}^{(l)}$ [2]. To use the FFT (the Fast Fourier Transform) with the Neumann condition $\frac{\partial \boldsymbol{u}}{\partial \boldsymbol{n}} = 0$, the function $f(x,y,z)$ defined in $0 \le x,y, \le L$ is expanded by using the relations

$$f(L+x,L+y,L+z) = f(L-x,L-y,L-z),\ f(x,y,z) = (x+2mL, y+2nL, z+2nL) \tag{23}$$

for integers k, m, and n. Setting the discrete differentiations to be

$$\begin{aligned} D_x f(x,y,z) &= \frac{1}{h} f(x+\frac{1}{2}h,y,z) - f(x-\frac{1}{2}h,y,z), \\ D_y f(x,y,z) &= \frac{1}{h} f(x,y+\frac{1}{2}h,z) - f(x,y-\frac{1}{2}h,z), \\ D_z f(x,y,z) &= \frac{1}{h} f(x,y,z+\frac{1}{2}h) - f(x,y,z-\frac{1}{2}h) \end{aligned} \tag{24}$$

for unit sampling step h, the Fourier transform of $\Delta f(x,y,z)$ is

$$FT\{\Delta f(x,y)\} = -\frac{4}{h^2}\left(\sin^2\frac{h}{2}\xi + 4\sin^2\frac{h}{2}\eta + +4\sin^2\frac{h}{2}\eta\right) F(\xi,\eta,\zeta), \tag{25}$$

where FTf expresses the Fourier transform of f, since

$$\begin{aligned} FT\{D_x f(x,y,z)\} &= \frac{2}{h} i \sin\frac{h}{2}\xi F(\xi,\eta,\zeta), \\ FT\{D_y f(x,y,z)\} &= \frac{2}{h} i \sin\frac{h}{2}\eta F(\xi,\eta,\zeta), \\ FT\{D_z f(x,y,z)\} &= \frac{2}{h} i \sin\frac{h}{2}\zeta F(\xi,\eta,\zeta). \end{aligned} \tag{26}$$

Therefore, we obtain the relation

$$(-\Delta)^\alpha f_{ijr} = IDFT\left\{\left(4\sin^2\frac{h}{2}k + 4\sin^2\frac{h}{2}m + 4\sin^2\frac{h}{2}n\right)^\alpha\right\} F_{kmn} \tag{27}$$

for discrete images f_{ij} and its discrete Fourier transform F_{mn}, where $IDFT$ expresses the inverse discrete Fourier transform.

3.3 Numerical Results

Figure 1 shows three-dimensional slices on the coronal, transverse, and sagittal planes. From left to right, Fig. 1 shows the three views of the original images, the flow fields computed by the Horn-Schunck method, and the flow fields computed by the deformable model. The three-dimensional flow field vector of each point is projected onto the plane, and the projected two-dimensional flow vector is expressed in the Middlebury Color Chart expression of vector field, which expresses directions and lengths of two dimensional vectors.

Since the Horn-Schunck and deformable model methods yield the piecewise constant flow field and piecewise affine flow field, respectively, the computational results by the former and latter methods are an over-smoothed field and the field shaped on the curved boundary, respectively.

Figure 2 shows α-map $\alpha^*(\boldsymbol{x})$, the optical flow field $\boldsymbol{u}^*(\boldsymbol{x},\alpha^*)$ which minimizes $F(\boldsymbol{u},\alpha;\kappa)$, and the solution of the two-path algorithm $\boldsymbol{u}^{**}$ from left to right.

Fig. 1. Three-dimensional optical flow fields. From left to right images flow fields computed by the Horn-Schunck method, the deformable-model method, on the coronal, transverse, and sagittal planes.

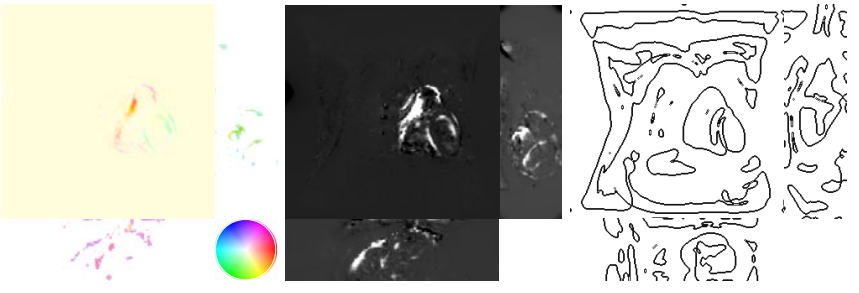

Fig. 2. Boundary surfaces on coronal, transverse, and sagittal planes. From left to right, color chart expression of optical flow field, norm of optical flow field, and the boundary surface line of the image. The boundary surface $\phi(x, y, z) = 0$ is extracted by a 3D version of Krueger's method [24]. $\phi(x, y, 0) = 0$, $\phi(x, 0, z) = 0$, and $\phi(0, y, z) = 0$ are illustrated.

Comparing with the boundary curves on planes,[2] our method clearly extracts the motion boundary. The result $\boldsymbol{u}^{**}$ is computed using the iteration

$$(\boldsymbol{I} + \frac{\Delta\tau}{\kappa}\boldsymbol{S}_{kmn})\boldsymbol{u}_{kmn}^{(l+1)} = \boldsymbol{u}_{kmn}^{(l)} + \Delta\tau(-\boldsymbol{\Lambda}^{2\alpha_{kmn}})\boldsymbol{u}_{kmn}^{(l)} - \frac{\Delta\tau}{\kappa}\boldsymbol{c}_{kmn},\ l \geq 0, \quad (28)$$

where α_{mn} is estimated as

$$\alpha_{kmn} = \min arg\{(\nabla f^{\top}\boldsymbol{u} + \partial_t f)^2 + \kappa(|T^{\alpha}u|^2 + |T^{\alpha}v|^2 + |T^{\alpha}w|^2)\} \quad (29)$$

[2] Setting f_G to be the convolution of the Gaussian with an appropriate variance and f, the segment boundary is the collection of points which satisfy $\nabla f_G^{\top}\boldsymbol{H}_G\nabla f_G = 0$ where $\boldsymbol{H}_G$ is the Hessian of f. For the boundary surface $\phi(x, y, z) = 0$, the boundary curves on the coronal, transverse, and sagittal planes are $\phi(x, y, 0) = 0$, $\phi(x, 0, z) = 0$, and $\phi(0, y, z) = 0$, respectively.

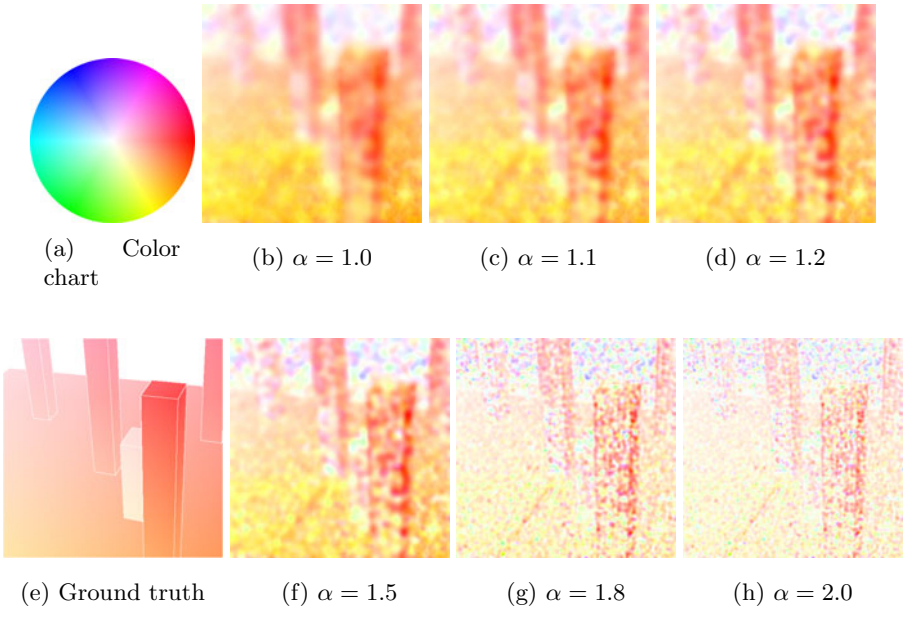

(a) Color chart (b) $\alpha = 1.0$ (c) $\alpha = 1.1$ (d) $\alpha = 1.2$

(e) Ground truth (f) $\alpha = 1.5$ (g) $\alpha = 1.8$ (h) $\alpha = 2.0$

Fig. 3. Computational results for $\lambda = \max|f|$. Results for $\alpha = 1.0, 1.1, 1.2, 1.5, 1.8,$ *and*2.0.

in the first step of the algorithm. These results show that the solution of the two-path algorithm detects the motion discontinuity caused on the motion boundary using the operation $\Lambda^{\alpha^*(\boldsymbol{x})}$.

Since we have no ground truth for the heart image sequence, we show the performance evaluation of the boundary detection using a two-dimensional image sequence with the ground truth.

Figure 3 shows the effect of the fractional order derivatives in the prior of the Horn-Schunck method. For $1 \leq \alpha \leq 2$, the method clearly detects the motion boundary.

Figures 4(d) and (h) are the results obtained by our method using the α-maps in Figs. 4(b) and (f). Setting $\boldsymbol{u}_T$ to be the ground truth fields, α_{true} is computed as

$$\alpha_{\text{true}} = \min arg\{(\nabla f^\top \boldsymbol{u}_T + \partial_t f)^2 + \kappa(|T^\alpha u|^2 + |T^\alpha v|^2 + |T^\alpha w|^2)\}. \quad (30)$$

Figures 4(b) and (f) show that the values of α-map on the motion boundaries are large, since for the description of motion fields on the motion boundaries, we are required to use higher order terms of eq. (15).

For the two-pass method, the results of the Horn-Schunck method are used as the initial estimation of the iteration algorithm. Figures 4(d) and (h) show that the boundaries of the sphere and blocks on the images are sharply extracted, since on the boundary, both the gray value of the image and the optical

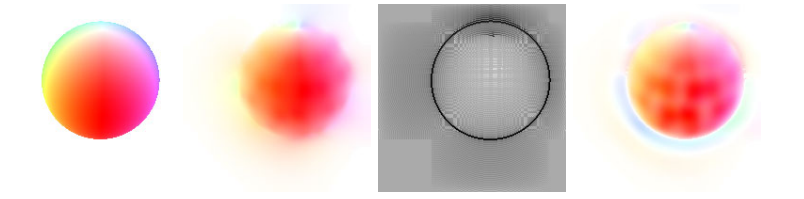

(a) Ground Truth (b) Horn-Schunck (c) α-map, $\kappa = 1.0$ (d) Tow-pass result

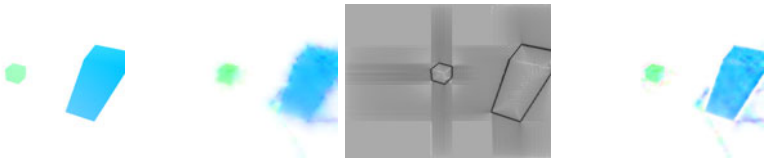

(e) Ground Truth (f) Horn-Schunck (g) α-map, $\kappa = 1.0$ (h) Tow-pass result

Fig. 4. Results: Rotating sphere and New marbled block. From left to right, motion field, α-map, the results of Horn-Schunck method, and results of the two-pass method. For the two-pass method, the results of the Horn-Schunck method are used as the initial estimation of the iteration algorithm.

flow process discontinuity in the gray-value topography and motion field, respectively. For both examples, the motion discontinuity on the segment boundaries is extracted by the fractional order optical flow.

3.4 Discussion

Setting $\{\boldsymbol{x}_k = (x_k, y_k, z_k)^\top\}_{k=1}^n$ and $\{t_k\}_{k=1}^n$ to be sets of sample points and sample values, respectively, the minimization of

$$J(f) = \sum_{k=1}^{n} (f(\boldsymbol{x}_k) - t_k)^2 + \kappa \int_\Omega |\Lambda^\alpha f|^2 d\boldsymbol{x} \tag{31}$$

where Ω is the define domain of the function $f(\boldsymbol{x})$, is a generalization [25] of the variational then-plate spline approximation. Here, the order α controls the continuity orders of the reconstructed function $f(x)$. We applied this property for the computation of volumetric cardiac optical flow field [6,7,1,25].

The result in Fig. 3 shows the flow fields which minimize

$$\begin{aligned} D(\boldsymbol{u}) &= \int_{\mathbf{R}^2} (\nabla f^\top \boldsymbol{u} + f_t)^2 dxdy + \kappa E_2(\boldsymbol{u}) \\ E_2(\boldsymbol{u}) &= \int \int_{\mathbf{R}^2} (|D^2 u|^2 + |D^2 v|^2 + |D^2 w|) dxdy, \end{aligned} \tag{32}$$

where

$$D^2 f = (f_{xx}, f_{xy}, f_{xz}, f_{xy}, f_{yy}, f_{yz}, f_{zx}, f_{zy}, f_{zz})^\top. \tag{33}$$

From the results in Figs 4 and 3, we observe the following properties on the boundary motion.

Observation 1. *If the motion of points in the neighborhood of the boundary is locally stationary, for instance, the motion is pure translation in a region, the projection of the ridge boundary moves elastically on the image. Therefore, the prior (regularizer) $E_2(\boldsymbol{u})$ of eq. (32) is suitable to detect the moving boundary.*

Observation 2. *If the motion of points in the neighborhood of the boundary on the image is nonstationary because of motion delay in the neighborhood, for instance, the delay in the global translation caused by local rotation, the projection of the ridge boundary moves viscoelastically on the image. Motion delay is expressed as a phase delay of the propagation of motion front. Therefore, the prior (regularizer)*

$$V(\boldsymbol{u}) = \int\int_{\mathbf{R}^3} (|\Lambda^{n+\varepsilon} u|^2 + |\Lambda^{n+\varepsilon} v|^2 + |\Lambda^{n+\varepsilon} w|^2) dxdy \tag{34}$$

for $0 < \varepsilon < 1$ is suitable to detect moving boundary.

For $\alpha = n + \varepsilon$ such that $0 < \varepsilon < 1$, the fractional order Laplacian is decomposed into the harmonic operation $(-\Delta)$ and fractional Laplacian $\Lambda^{2\varepsilon} = (-\Delta)^\varepsilon$. This decomposition can be read that $\Lambda^{2\alpha} f$ is achieved by applying the harmonic operation $(-\Delta)^n$ to $g = (-\Delta)^\varepsilon f$, which is achieved by convolution between the function f and the Riesz potential [23]. Numerical filtering of the operation $(-\Delta)^\varepsilon$ derived in eq.(27) possesses a smoothing effect to the optical flow field $\boldsymbol{u}^{(l)}$ in each step of iteration. Therefore, our numerical scheme generates a smoothed optical flow before applying the harmonic operation. This presmoothing property of the numerical scheme yields a better performance for $\alpha = n + \varepsilon$ such that $0 < \varepsilon < 1$.

Our method estimates the continuity order of the optical flow field. Furthermore, as shown in the results, our method also extracts a higher order optical flow if the gray-value distribution of an image is discontinuous. The results mathematically provide a method to estimate the local continuity order of the optical flow field, and theoretically shows that for motion boundary extraction and tracking, the prior with higher order differentiation is preferable. For the tracking of the image of an elastic boundary of a ridged object in space, the order of the differentiation is two. If the optimal order of the points is between 1 and 2, the points are viscoelastically moving [16,17] on an image. The results lead to the conclusion that using the local continuity order, it is possible to extract the motion boundary and separate moving segments from the background.

4 Concluding Remarks

The order of differentiation in the prior decides the continuity order of the optical flow field. Therefore, our results show that orders between one and two

are preferable to detect discontinuity optical flow vectors, which appear on the motion boundary. Although TV regularization [12,13] accurately and stably computes an optical flow field and extracts moving segments from the background, the operation is nonlinear. The results leads to the conclusion that using the local continuity order, it is possible to extract the motion boundary and separate moving segments from the background.

This research was supported by "Computational anatomy for computer-aided diagnosis and therapy: Frontiers of medical image sciences" funded by Grant-in-Aid for Scientific Research on Innovative Areas, MEXT, Japan, Grants-in-Aid for Scientific Research founded by Japan Society of the Promotion of Sciences, Research Fellowship for Young Scientist founded by Japan Society of the Promotion of Sciences, and Research Associate Program of Chiba University. Y. Kameda is supported as a Research Fellow of the Japan Society for the Promotion of Science, The heart image sequence is provided from Robarts Research Institute at the University of Western Ontario through Prof. John Barron.

References

1. Sorzano, C.Ó.S., Thévenaz, P., Unser, M.: Elastic registration of biological images using vector-spline regularization. IEEE Tr. Biomedical Engineering 52, 652–663 (2005)
2. Davis, J.A., Smith, D.A., McNamara, D.E., Cottrell, D.M., Campos, J.: Fractional derivatives-analysis and experimental implementation. Applied Optics 32, 5943–5948 (2001)
3. Zhang, J., Wei, Z.-H.: Fractional variational model and algorithm for image denoising. In: Proceedings of 4th International Conference on Natural Computation, vol. 5, pp. 524–528 (2008)
4. Oldham, K.B., Spanier, J.: The Fractional Calculus: Theory And Applications of Differentiation and Integration to Arbitrary Order, Dover Books on Mathematics. Dover, New York (2004)
5. Podlubny, I.: Fractional Differential Equations. An Introduction to Fractional Derivatives, Fractional Differential Equations, Some Methods of Their Solution and Some of Their Applications. Academic Press, London (1999)
6. Suter, D.: Motion estimation and vector spline. In: Proceedings of CVPR 1994, pp. 939–942 (1994)
7. Suter, D., Chen, F.: Left ventricular motion reconstruction based on elastic vector splines. IEEE Tr. Medical Imaging, 295–305 (2000)
8. Nagel, H.-H., Enkelmann, W.: An investigation of smoothness constraint for the estimation of displacement vector fields from image sequences. IEEE Trans. on PAMI 8, 565–593 (1986)
9. Horn, B.K.P., Schunck, B.G.: Determining optical flow. Artificial Intelligence 17, 185–204 (1981)
10. Timoshenko, S.P.: History of Strength of Materials. Dover, New York (1983)
11. Grenander, U., Miller, M.: Computational anatomy: An emerging discipline. Quarterly of Applied Mathematics 4, 617–694 (1998)
12. Papenberg, N., Bruhn, A., Brox, T., Didas, S., Weickert, J.: Highly accurate optic flow computation with theoretically justified warping. IJCV 67, 141–158 (2006)

13. Yin, W., Goldfarb, D., Osher, S.: A comparison of three total variation based texture extraction models. J. Visual Communication and Image Representation 18, 240–252 (2007)
14. Eckstein, J., Bertsekas, D.P.: On the Douglas-Rachford splitting method and the proximal point algorithm for maximal monotone operators. Mathematical Programming 55, 293–318 (1992)
15. Modersitzki, J.: Numerical Methods for Image Registration. Oxford Univ. Pr., Oxford (2004)
16. Momani, S., Odibat, Z.: Numerical comparison of methods for solving linear differential equations of fractional order. Chaos, Solitons and Fractals 31, 1248–1255 (2007)
17. Murio, D.A.: Stable numerical evaluation of Grünwald-Letnikov fractional derivatives applied to a fractional IHCP. Inverse Problems in Science and Engineering 17, 229–243 (2009)
18. Debbi, L.: Explicit solutions of some fractional partial differential equations via stable subordinators. J. of Applied Mathematics and Stochastic Analysis, Article ID 93502 2006, 1–18 (2006)
19. Debbi, L.: On some properties of a high order fractional differential operator which is not in general selfadjoint. Applied Mathematical Sciences 1, 1325–1339 (2007)
20. Chechkin, A.V., Gorenflo, R., Sokolov, I.M.: Fractional diffusion in inhomogeneous media. J. Phys. A: Math. Gen. 38, L679–L684 (2005)
21. Duits, R., Felsberg, M., Florack, L.M.J., Platel, B.: α scale spaces on a bounded domain. In: Griffin, L.D., Lillholm, M. (eds.) Scale-Space 2003. LNCS, vol. 2695, pp. 502–518. Springer, Heidelberg (2003)
22. Papenberg, N., Bruhn, A., Brox, T., Didas, S., Weickert, J.: Highly accurate optic flow computation with theoretically justified warping. IJCV 67, 141–158 (2006)
23. Ortiguera, M.D.: Riesz potential operations and inverses via fractional centred derivatives. International Journal of Mathematics and Mathematical Sciences, Article ID 48391, 1–12 (2008)
24. Krueger, W.M., Phillips, K.: The geometry of differential operator with application to image processing. PAMI 11, 1252–1264 (1989)
25. Unser, M., Blu, T.: Fractional spline and wavelets. SIAM Review 43, 43–67 (2000)